Arctic Science

OPEN ACCESS | Research Article

Exploring the impact of surface lapse rate change scenarios on mountain permafrost distribution in four dissimilar valleys in Yukon, Canada

Madeleine C. Garibaldi[a], **Philip P. Bonnaventure**[a], **Nick C. Noad**[a], **and Will Kochtitzky**[b]

[a]Department of Geography and Environment, University of Lethbridge , Lethbridge, AB T1K 3M4, Canada; [b]School of Marine and Environmental Programs, University of New England , Biddeford, ME 04005, United States

Corresponding author: **Madeleine C. Garibaldi** (email: madeleine.garibaldi@uleth.ca)

Abstract

A scenario-based approach was used to test air and ground response to warming with and without changes to inverted surface lapse rates in four Yukon valleys. Generally, climate warming coupled with weakening of temperature inversions resulted in the greatest increase in air temperature at low elevations. However, ground temperatures at high elevations showed the greatest response to warming and variability between scenarios due to increased connectivity between air and ground. Low elevations showed less of a response to warming and permafrost was largely preserved in these locations. Local models also predicted higher permafrost occurrence compared to a regional permafrost probability model, due to the inclusion of differential surface and thermal offsets. Results show that the spatial warming patterns in these mountains may not follow those predicted in other mountain environments following elevation-dependent warming (EDW). As a result, the concept of EDW should be expanded to become more inclusive of a wider range of possible spatial warming distributions. The purpose of this paper is not to provide exact estimations of warming, but rather to provide hypothetical spatial warming patterns, based on logical predictions of changes to temperature inversion strength, which may not directly follow the distribution projected through EDW.

Key words: TTOP model, permafrost, Yukon, surface lapse rate, elevation-dependent warming

1. Introduction

The distribution of mountain permafrost is complex owing to the extreme spatial variability in surface and near surface characteristics, including incoming solar radiation, elevation, slope, snow cover, vegetation, and soil moisture (Shur and Jorgenson 2007; Gruber and Haeberli 2009). Generally, however, there are two main distribution patterns based on the change in mean annual air temperature (MAAT) with elevation. First, in low latitude or maritime mountain ranges, permafrost is generally assumed to be present at high elevations and absent at low elevations, following the spatial topographic distribution of MAAT cooling with increased elevation (Guglielmin et al. 2003; Boeckli et al. 2012; Bonnaventure et al. 2012). With warming climate, permafrost in these environments is expected to warm and thaw unidirectionally, with the lower elevation limit of permafrost moving upslope (Harris et al. 2009; Bonnaventure and Lewkowicz 2013). In these environments, warming is also expected to be amplified at higher elevations due to a variety of mechanisms including changes in albedo, changes in water vapor and latent heat release and aerosols (Pepin et al. 2015). This phenomenon is referred to as elevation-dependent warming (EDW) and has been supported by observations and climate modelling studies in the Andes, Rocky Mountains, and Alps and for certain elevations of the Qinghai-Tibet Plateau (Minder et al. 2018; Aguilar-Lome et al. 2019; Palazzi et al. 2019; Li et al. 2020; Williamson et al. 2020; Zhang et al. 2023). However, this concept and observations have only been made in regions with normal, linear relations between air temperature and elevation (Bonnaventure and Lewkowicz 2011; Rangecroft et al. 2016; Deluigi et al. 2017). As a result, the concept of EDW is already thought to be non-inclusive for certain mountain environments including areas of the Qinghai-Tibet Plateau, likely due to the lack of elevation dependent temperature trends (You et al. 2010; Li et al. 2020; Zhang et al. 2023).

A second mountain permafrost distribution pattern is more commonly found in high-latitude, continental mountains, whereby permafrost is present in both valley bottoms and high elevations because of persistent winter temperature inversions (Bonnaventure and Lewkowicz 2011; Lewkowicz and Bonnaventure 2011; Bonnaventure et al. 2012; Noad and Bonnaventure 2022). These inversions produce warming air temperatures with increasing elevation up to treeline or higher, resulting in the highest air temperatures at mid to high elevations. In such locations the surface lapse rate (SLR) or change in temperature with elevation, is said to be

inverted. With warming MAAT, this permafrost distribution pattern and the complicated relation between temperature and elevation may not produce the same warming and thawing pattern as in locations with a linear permafrost distribution. As shown for portions of Yukon subject to inverted SLRs below treeline, warming results in a bidirectional loss of permafrost as thaw advances both up and downslope from treeline (Bonnaventure and Lewkowicz 2013). However, previously only uniform changes in MAAT have been applied and potential changes in the strength of the inverted SLR were not considered (Bonnaventure and Lewkowicz 2013). Based on downscaled climate reanalysis data, MAATs over the past two decades (1981–2021) for parts of central and southeast Yukon have risen by 0.4–0.5 °C per decade with the greatest warming rate occurring in winter and autumn (Wang et al. 2016). With climate change, winter inversions over larger portions of the Arctic are expected to weaken (become more normal), although there is limited consensus on how surface-based inversions (SBIs) might change (Koenigk et al. 2013; Hou and Wu 2016; Ruman et al. 2022). This further complicates spatial and elevation warming distribution of both the air and the ground. As a result, EDW may not hold true in the high-latitude, continental mountains due to the presence of persistent inverted SLRs.

The objectives of this paper were to theoretically examine how changes in inverted SLR strength may alter or offset warming potential related to EDW in four dissimilar high-latitude, continental mountain valleys in Yukon. This was done using a scenario-based approach to examine the logical possibilities for responses in warming (based solely on warming and altered SLRs) in both the air and ground thermal regime, as the exact changes in SLR for this region remain undetermined. The results of this study should provide an evaluation of the reliability and direct transferability of the conclusions derived from EDW both in the high-latitude, continental mountains of Yukon, but also in other locations subject to strong winter temperature inversions.

2. Study area

Four valleys with unique temperature inversions strengths, surface characteristics and spatial distributions of the air and ground thermal regimes in Yukon were selected, two along the Dempster Highway and two along the North Canol Road (Fig. 1). The study areas along the Dempster Highway in the Ogilvie Mountains are called Valley Dempster South (Valley DS) and Valley Dempster North (Valley DN), while the sites along the North Canol in the Selwyn Mountains are named Mile 222 Valley (Valley M222) and MacMillan Transect South Valley (Valley MTS). These valleys were primarily selected based on their distinct characteristics and the existence of fine resolution models of the air and ground thermal regime in addition to spatial maps for each of the TTOP model parameters under current conditions. These would allow for scenario-based changes in air temperature and SLRs to assess the potential response in the air and ground thermal regime accounting for spatial differences in surface and thermal offsets.

The Ogilvie Mountains have remained unglaciated since the Pre Reid Glaciation and are mainly comprised of narrow valleys with moderate relief, surface deposits of colluvium and low to moderate segregated and wedge ice (Yukon Ecoregions Working Group 2004; Burn et al. 2015; O'Neill et al. 2019.). The climate is considered to be Subarctic continental, with moderate precipitation amounts mainly falling as rain in the summer (Yukon Ecoregions Working Group 2004). Contrastingly, the Selwyn Mountains have been extensively glaciated, resulting in a high elevation range compared to the Ogilvie Mountains, and still have local alpine glaciers (Bostock 1966; Yukon Ecoregions Working Group 2004). Additionally, these mountains receive some of the highest precipitation amounts in Yukon outside of the Pacific Maritime region (Yukon Ecoregions Working Group 2004). This heavy amount of snowfall prevents the establishment of continuous permafrost in this region. Large accumulations of glacial sediments are only present in the bottoms of major valleys while the upper slopes and smaller valleys are composed of Holocene colluvium (Yukon Ecoregions Working Group 2004). Lastly, this region is expected to have low to moderate segregated ice and negligible wedge ice (O'Neill et al. 2019).

Valley DS is the southernmost site in the Ogilvie Mountains, located about 43 km south of the Engineer Creek Territorial Campground. It is an east oriented valley, which is treed on one slope and treeless on the other slope (Fig. 2).

Valley DS has an elevation range of about 700 m. Based on previous models, the average annual mean air temperature (AMAT) over the valley is –6.4 °C (2019–2021) with the coldest temperatures found in the valley bottom and the warmest around treeline or high elevations (Garibaldi et al. 2024). The valley is considered to be underlain by continuous permafrost; however, recent models have shown it is likely to have discontinuous permafrost (Heginbottom 1995; Bonnaventure et al. 2012; Garibaldi et al. 2024). Additionally, average annual mean ground temperature (AMGT) was modelled to be –1.6 °C (2019–2021), with permafrost present in both the valley bottom and at high elevations (Garibaldi et al. 2024).

Valley DN is the northern most site and, despite being only 10 km away from Valley DS, is quite different in terms of vegetation. Valley DN is a treeless valley, with vegetation consisting of moss and lichen on the valley floor with a few scattered shrubs and scree slopes (Fig. 2). This valley has a north orientation. The elevation range in this valley is about 520 m. As in Valley DS, the strong temperature inversions in this valley result in the coldest AMATs in the valley bottom while the warmest are at the highest elevations due to SLRs remaining inverted or only gently normal to the ridgetops. Average AMAT over the valley was modelled to be –5.1 °C (2012–2021) (Garibaldi et al. 2024). This valley is also considered to be in the continuous permafrost zone, which is supported by recent local modelling (Heginbottom 1995; Garibaldi et al. 2024). Average AMGT was modelled to be –2.1 °C (2019–2021) with permafrost only predicted to be absent in deeply incised channels at mid elevations on the east facing slope.

Valley Mile 222 is located on the North Canol Highway near the Yukon/Northwest Territories border in a wide valley. The dominant vegetation is dwarf birch in the lower portions of

Fig. 1. Map showing the locations of the four study area valleys. Permafrost layer from Brown et al. (2002). The smaller maps show the locations of the air and ground surface temperature stations within each valley. Colours for the air temperature stations indicate the year of installation. Base layer from DigitalGlobe Inc. (Imagery © [2017]). Contains information licenced under the Open Government Licence—Canada. Contains information licenced under the Open Government Licence—Yukon. Contains information from the United States Census Bureau.

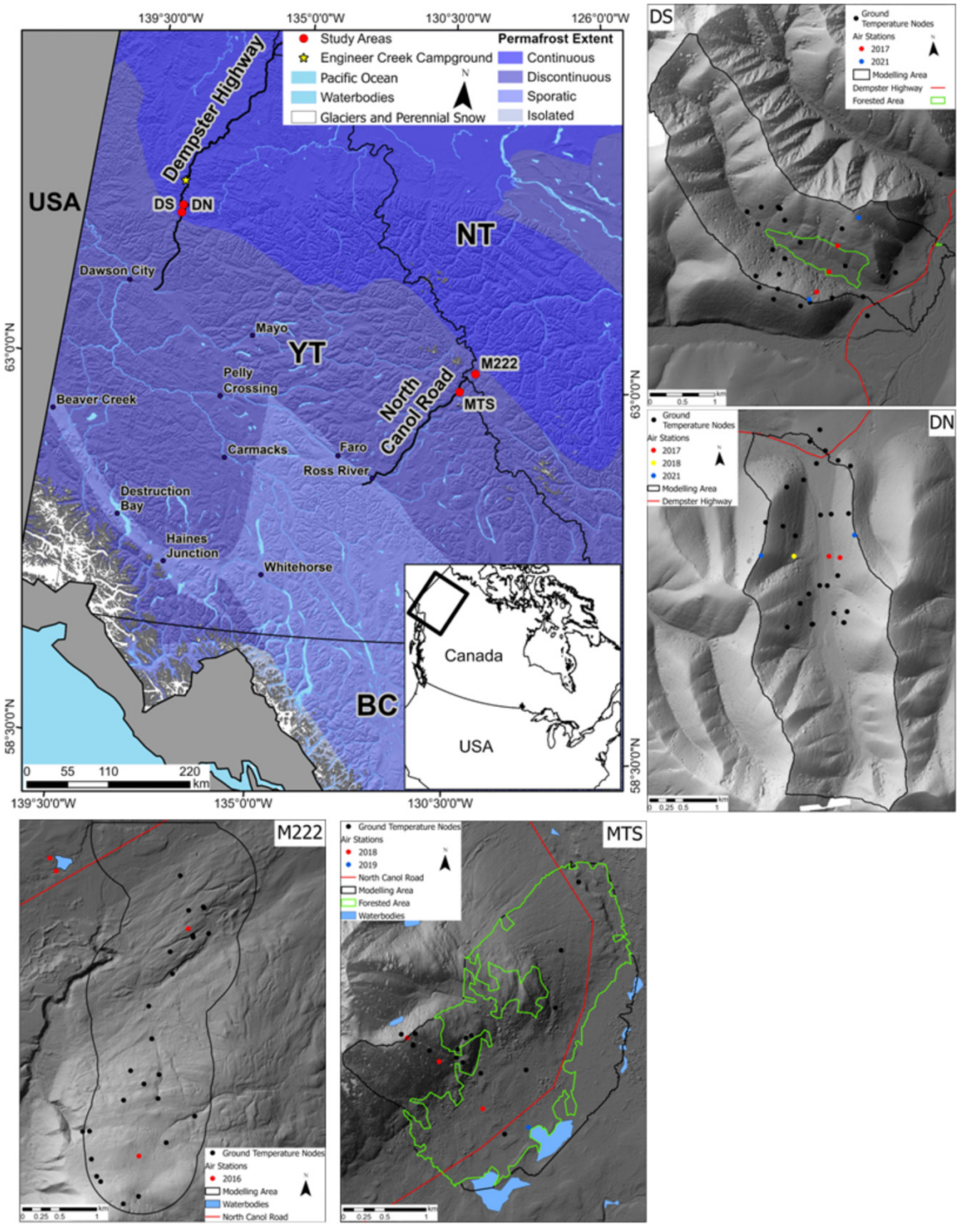

the valley, transitioning to predominately mosses and lichens at higher elevations (Fig. 2). AMAT was predicted to be –6.2 °C (2019–2021) over the valley, with the coldest temperatures also predicted in the valley bottoms and the warmest at mid elevations. Despite the comparably cold air temperatures, permafrost was modelled to underlay only a small portion of the valley, likely due to the high amount of snow and shrub dominant vegetation keeping the ground warm during winter. As a result, AMGT over the valley was modelled to be 0.3 °C (2019–2021). This valley was considered to be under-

Fig. 2. Site photos for each of the four valleys. (A) Photo facing southeast at Valley DS showing the treed and treeless slopes of the valley, taken on August 14, 2018. (B) Photo facing south at Valley DN showing the limited vegetation in the valley bottom and bare slopes, taken on August 14, 2018. (C) Photo facing southeast at Valley M222 showing the shrub dominant vegetation and limited relief, taken on August 17, 2019. (D) Photo facing southwest of Valley MTS, showing the forested valley bottom and lower slope transitioning to alpine tundra, taken on August 22, 2019. Photo Credit: Madeleine Garibaldi.

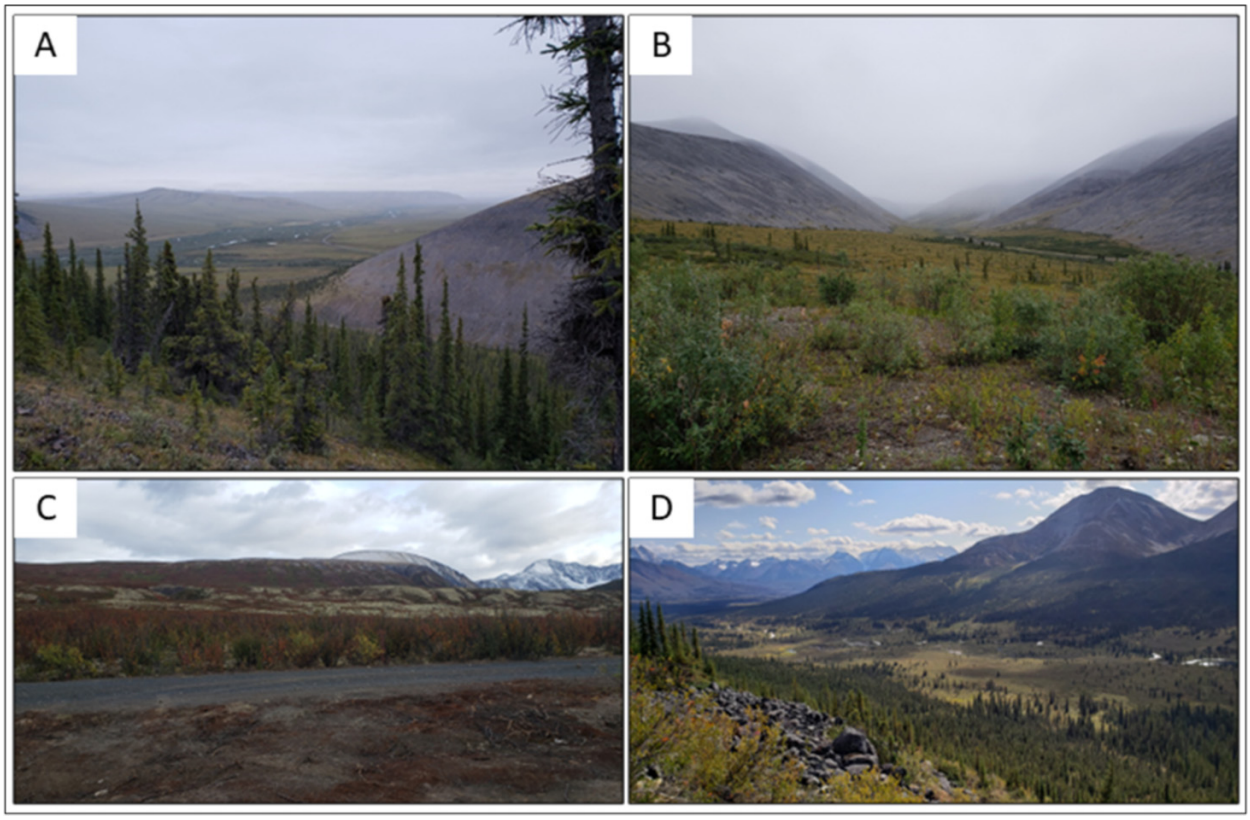

lain by extensive discontinuous permafrost in circumpolar models but was more likely to be underlain by sporadic discontinuous permafrost (Heginbottom 1995; Garibaldi et al. 2024).

Lastly, Valley MTS is the southernmost site located on the North Canol and amongst the study areas overall. This site has the largest elevation range of the study areas (about 805 m) and is comprised of treed slopes that transition to alpine tundra, consisting of moss, lichen, and scree slopes at high elevations. AMAT was modelled to be –5.1 °C (2019–2021) with the coldest air temperatures in the valley bottom and the warmest at treeline due to the annually inverted SLR. This valley is also deemed to be in the extensive discontinuous permafrost zone and local modelling predicted average AMGT to be –0.3 °C (2019–2021) (Heginbottom 1995; Garibaldi et al. 2024).

3. Methods

3.1. Current air and ground model development

The models for current air temperature metrics were created using in situ data from at least three air temperature stations in each valley and the associated elevations (2019–2021) (Table S1). SLRs were calculated and AMAT was spatially modelled using a 2 m digital elevation model (DEM) (Imagery © [2017] DigitalGlobe, Inc.):

$$\text{SLR} = \frac{T_2 - T_1}{E_2 - E_1} \quad (1)$$

where T is the daily average air temperature (°C) and E (m) is the elevation. AMGST and AMGT were spatially modelled using the temperature at top of permafrost (TTOP) model (Smith and Riseborough 2002):

$$\text{TTOP} = \frac{(rk * n_t * TDD_a) - (n_f * FDD_a)}{P} \; for \; \text{TTOP} \leq 0$$
$$\text{TTOP} = \frac{(n_t * TDD_a) - (\frac{1}{rk} * n_f * FDD_a)}{P} \; for \; \text{TTOP} > 0 \quad (2)$$

where rk is the ratio of thawed to frozen thermal conductivity of the substrate, n_f and n_t are freezing and thawing N-factors, FDD_a and TDD_a are freezing and thawing degree days in the air (°C-days), and P is the period (365 days). Each of the TTOP model parameters were calculated and related spatially to topographically derived variables and vegetation classes. First, FDD_a and TDD_a at each air temperature station were calcu-

lated:

$$\text{FDD} = |\sum_{1}^{P} T|, T < 0 \quad \text{TDD} = |\sum_{1}^{P} T|, T > 0 \tag{3}$$

where T is the daily average temperature (°C) and P is the period (365 days). This equation can be used to calculate freezing and thawing degree days in the air (a) or ground surface (s). The changes in FDD_a and TDD_a with elevation were then determined, and the 2 m DEM was used to spatially model this change:

$$\Delta\text{DD} = \frac{DD_2 - DD_1}{E_2 - E_1} \tag{4}$$

where DD (°C-days) are either the freezing or thawing degree days and E (m) is the corresponding elevation. N-factors for the approximately 25 ground temperature nodes (GTN) (sites recording ground surface temperature) in each valley (Table S1) were then calculated using the modelled FDD_a and TDD_a for each site and the measured freezing and thawing degree days at the ground surface (FDD_s and TDD_s):

$$n_f = \frac{FDD_s}{FDD_a} \text{ and } n_t = \frac{TDD_s}{TDD_a} \tag{5}$$

The N-factors were then spatially modelled using Empirical Bayesian Kriging (EBK) and several topographically derived and spatial biological variables including aspect and/or potential incoming solar radiation (PISR), topographic position index (TPI), and vegetation class. Lastly, *rk* was spatially derived based on measured values at the stations located in each valley and assigned using vegetation class, elevation, and topographic wetness. The additional details for the model creation and locations of the observation instruments can be found in Garibaldi et al. (2024) and additional information on the derivation of *rk* and observation instrument metadata can be found in the supplemental data (Tables S1 and S2).

3.2. Surface lapse rate changes and climate change scenarios

To assess the potential outcomes of warming and evaluate an alternative to EDW in this region, several potential scenarios were run including both baseline warming coupled with current SLR conditions and weakening of the inverted SLRs in each valley. Using the location of the lowest air station, the baseline magnitude of warming was determined for the shared socioeconomic pathway (SSP) 2–4.5 for the 2071–2100 climate normal using ClimateNA (Wang et al. 2016; IPCC 2022; Mahony et al. 2022). A radiative forcing of 4.5 was selected as it is frequently used in climate change studies (Nitzbon et al. 2020; Soong et al. 2020; Garibaldi et al. 2022; Ruman et al. 2022). To determine the magnitude of warming, the difference between MAAT for the downscaled current climate (1981–2010) and the predicted MAAT for each climate warming scenario was added to the measured AMAT for the valley (Table 1). This was done to account for discrepancies between the downscaled climate normal and the measured air temperatures in each valley. For the first warming scenario, only the uniform warming was applied and the SLRs were held at the measured current values. For the subsequent scenarios, the annual inverted SLRs were weakened by 1 and 5 °C km^{-1} in addition to the baseline warming. The baseline warming was applied in two different ways. First, the warming was applied to the measured AMAT at the lowest elevation air station in each valley and the change in SLR was applied from the same elevation. Second, the warming was applied to the air station at the mid elevation and the change in SLR was applied from this elevation. This was to prevent the overall warming in each valley from exceeding that predicted in each SSP scenario.

Table 1. Magnitude of the baseline change in MAAT, FDD_a, and TDD_a for each valley for the shared socioeconomic pathway (SSP) 2–4.5 scenario 2071–2100 climate normal (Mahony et al. 2022).

	ΔMAAT (°C)	Δ FDD_a (°C days)	ΔTDD_a (°C days)
Valley DS	+3.1	−662	+326
Valley DN	+3.1	−687	+312
Valley M222	+2.4	−478	+297
Valley MTS	+2.4	−468	+318

The TTOP model was used to determine the resulting changes to the ground thermal regime in response to warming air temperatures (eq. 2) (Smith and Riseborough 2002). For this study, spatial models of n_f, n_t, and *rk* developed for current conditions were utilized (Garibaldi et al. 2024). To determine the baseline magnitude of change in both FDD_a and TDD_a, the same method as for MAAT was utilized, where the difference between the downscaled climate data for the 1981–2010 climate normal and the values from each climate change scenario from ClimateNA were added to the spatial models for the current climate. As only changes to the winter inverted SLRs are expected with climate change (Ruman et al. 2022), only the change in FDD_a with elevation was adjusted. First, the proportion of the year with daily average temperatures below 0 °C was determined for each valley (60%). Then the freezing season SLR was determined by increasing the annual SLR (1 or 5 °C km^{-1}) by 60%. Theoretical FDD_a for a specified elevation was then calculated using measured air temperatures in the valley bottom and the adjusted freezing season SLR (eqs. 1, 3, and 4). Since the inversions are primarily a freezing season or winter phenomenon (Zhang et al. 2011; Noad and Bonnaventure 2022), only a uniform change in TDD_a was used with no adjustment to the change in TDD_a with elevation. For each scenario, only inverted SLRs were weakened. If the SLR was strongly normal (>3.0 °C km^{-1}), the SLR and FDD_a were kept the same and only the uniform warming was applied. The new FDD_a, and TDD_a and SLRs were then used in conjunction with a 2 m DEM (Imagery © [2017] DigitalGlobe, Inc.) to spatially model the new FDD_a and TDD_a distribution. These surfaces, in addition to the original n_f, n_t, and *rk* surfaces, were then used as inputs in the TTOP model to determine the new spatial distribution of the ground thermal regime. Cells determined to be above 0 °C were recalculated using the TTOP model equation for seasonal frost.

Table 2. Current and perturbed SLRs for each valley used in the different warming scenarios.

	Slope	Current SLR (°C km^{-1})		−1 SLR (°C km^{-1})		−5 SLR (°C km^{-1})	
Valley DS	NE Facing	8.0	*0.5*	7.0	*−0.5*	3.0	*−4.5*
	SW Facing	11.7	*−0.9*	10.7	*−1.9*	6.7	*−5.9*
Valley DN	E Facing	3.5	*−0.1*	2.5	*−1.1*	−1.5	*−5.1*
	W Facing	7.1	*1.3*	6.1	*0.3*	2.1	*−3.7*
Valley M222	NA	5.9	*−2.7*	4.9	*−2.7*	0.9	*−2.7*
Valley MTS	NA	10.6	*−5.1*	9.6	*−5.1*	5.6	*−5.1*

Note: Italicized values are the upper elevation SLRs.

The models with baseline warming initiated at the valley bottom provided average warming most similar to that predicted in the downscaled climate reanalysis data. When baseline warming was initiated at the mid elevation station coupled with changes in the inversion strength, the resulting model had an average predicted warming across the valley that exceeded the predictions of the downscaled climate data.

4. Results

4.1. Changes in inversion strength

In valleys with highly inverted SLRs at lower elevations, even a 5 °C weakening still resulted in annual inverted SLRs in these portions of the valleys (Table 2). The only exception to this was the lower east facing side of Valley DN, where the SLR became normal annually with a 5 °C km^{-1} weakening. Additionally, as some of the upper SLRs were only slightly inverted, even small decreases in inversion strength resulted in a change from an annually inverted SLR to a normal SLR. For SLRs at high elevations, which are currently normal, decreasing winter inversions produced an even stronger normal annual SLR, resulting in decreasing air temperature with increasing elevation.

This also held true for changes in FDD_a with elevation as the strong winter inversions present in the lower portions of each valley resulted in a decrease in the number of FDD_a with increasing elevation, even with a 5 °C km $^{-1}$ weakening of the annual inverted SLR. Although the annual SLR for the lower portion of the east facing side of Valley DN became normal with changes to the inversion strength, FDD_a continued to decrease with increasing elevation in all of the valley bottoms except Valley M222. Additionally, like the annual SLRs at higher elevations weakening of the inversions resulted in increasing FDD_a with increasing elevation.

4.2. Potential changes in the spatial distribution of air temperature

In all four valleys a uniform warming scenario without changes in the SLR, MAAT was predicted to warm evenly, maintaining the current spatial distribution pattern of air temperatures. As a result, under this warming scenario, the highest air temperatures in Valley DS were still predicted at mid elevations around treeline on the southwest facing slope (Fig. 3). At Valley DN, the highest air temperatures were predicted at high elevations especially on the west-facing slope similar to the current spatial distribution (Fig. 3). The highest air temperatures at Valley M222 were still predicted at mid elevations while the coldest temperatures predicted at the highest elevations (Fig. 3). Lastly, at Valley MTS, the highest MAAT were also still predicted at mid elevations, corresponding to treeline (Fig. 3). However, scenarios involving a uniform warming coupled with a change in SLR strength, altered the spatial distribution of air temperature with elevation, as high elevations were predicted to warm less relative to temperatures at mid and low elevations and substantially less than the average warming rate from ClimateNA (Fig. 4). Additionally, due to the reduced warming at high elevations resulting from more gently inverted SLRs or even a transition to normal SLRs, average warming over the valleys was also less than predicted from ClimateNA (Table 3). This reduction in overall warming increased with decreasing inverted SLR strength, becoming most pronounced for the 5 °C km^{-1} weakened SLR scenario. The magnitude of this reduction was dependent on the strength of the lower inverted SLR and the magnitude and sign (normal or inverted) of the higher elevation SLR.

In Valleys DS, DN and MTS, SLRs from low to mid elevations remained strongly inverted (SLR > 3.0 °C km^{-1}) even with a 5 °C km^{-1} reduction, while the SLR above the mid elevations switched from inverted to normal (or remained normal), causing the largest change in temperature in the valley bottom and reducing warming at high elevations. At Valley M222 under a 5 °C km^{-1} decrease in inverted SLR strength, the SLR remained only slightly inverted (<1 °C km^{-1}). This resulted in air temperatures in the valley bottom remaining only slightly colder than those at mid elevations and a small difference in the rate of warming across the valley. Overall, the changes in the spatial distribution of warming and MAAT, specifically the disproportionately less warming at high elevations under reduced inverted SLR strength, highlights how changes in SLRs may completely or partially offset warming by EDW drivers at these locations.

4.4. Potential changes in the distribution of ground temperature

Despite uniform warming across the valley or greater warming at low elevations (depending on the SLR scenario), MAGT warmed the most at high elevations for all but the 5 °C km^{-1} reduction in inverted SLR strength for Valleys DS, DN, and MTS. Under this scenario, MAGT at high elevations warmed relatively little compared to temperatures in the valley bottom (Valley DS and Valley DN) or mid elevations (Valley MTS). In Valley M222, the warming pattern in MAGT differed from the other valleys with MAGT predicted to warm the most at high elevations for all scenarios. However, despite greater warming at higher elevations generally in each valley, the relative MAGT distribution differed. In Valley DS, the relatively cold MAGTs were predicted for all scenarios in the valley bottom and at high elevations (Fig. 5). This was also true in Valley DN, where the coldest temperatures were predicted on the west-facing slope and in a small portion of the

Fig. 3. Spatial distribution of mean annual air temperature (MAAT) in each of the valleys for current conditions and for the SSP 2–4.5 2071–2100 climate normal assuming no change in the surface lapse rate (SLR), a 1 °C km^{-1} weakening of the inverted SLR, and a 5 °C km^{-1} weakening of the inverted SLR. Base layer from DigitalGlobe Inc. (Imagery © [2017]). Contains information licenced under the Open Government Licence—Canada.

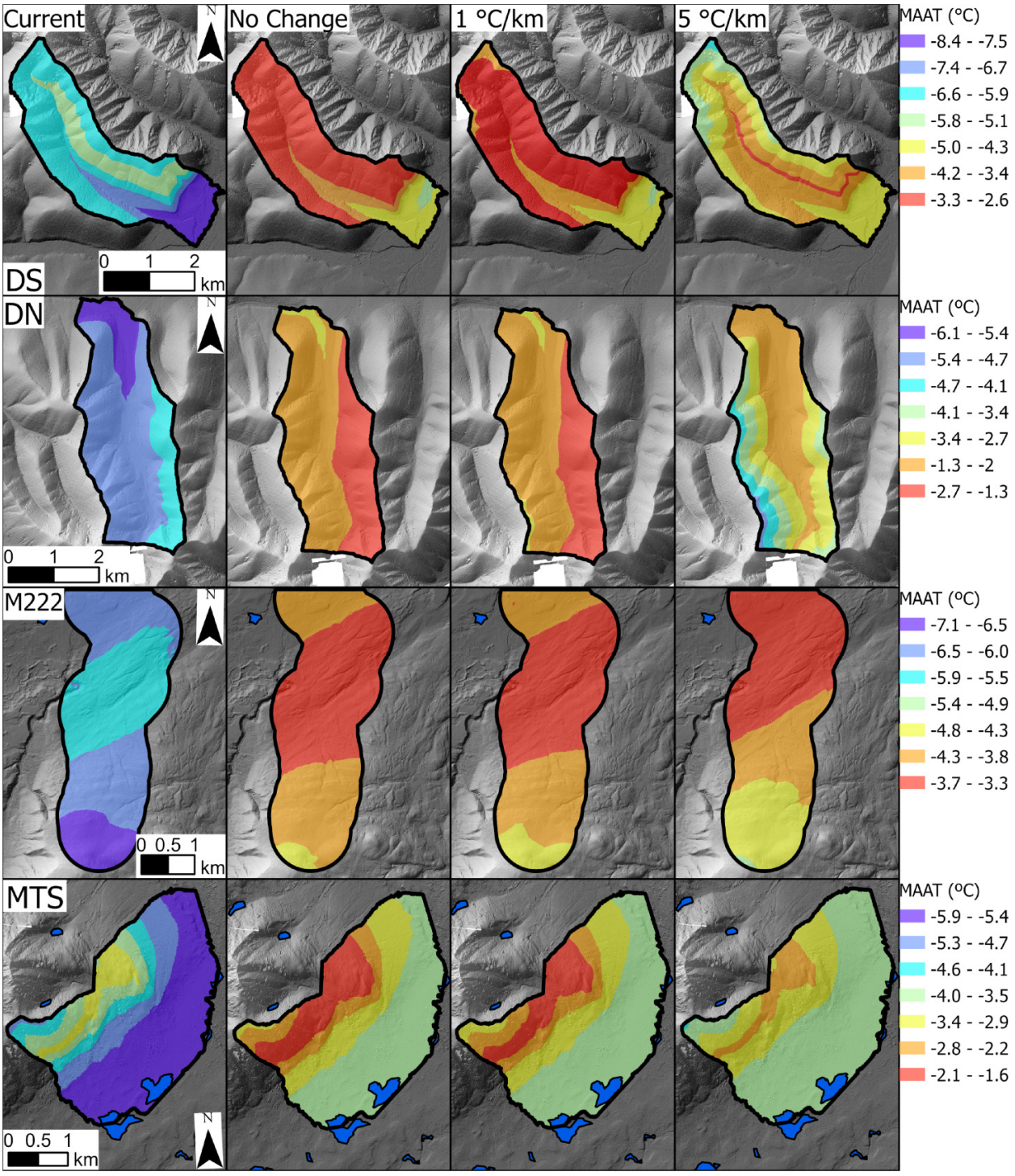

valley bottom (Fig. 5). In Valley M222, the coldest MAGT were modelled at high elevations and the warmest in the valley bottom (Fig. 5). Lastly, in Valley MTS, MAGT in the valley bottom remained the coldest throughout each warming scenario (Fig. 5).

Overall, MAGT in the valley bottom remained relatively cold for all scenarios while MAGT at high elevations varied depending on the warming scenario. As a result, the percentage of each valley underlain by near surface permafrost (NSP) was highest for the 5 °C km^{-1} weakened inverted SLRs as

Fig. 4. Spatial distribution for the rate of warming (°C per decade) following a 5 °C km^{-1} weakening of the inverted surface lapse rates (SLR) for (A) Valley DS, (B) Valley DN, (C) Valley M222, and (D) Valley MTS. Average warming rate (°C per decade) across each valley from ClimateNA is also given (Wang et al. 2016; Mahony et al. 2022). Base layer from DigitalGlobe Inc. (Imagery © [2017]). Contains information licenced under the Open Government Licence—Canada.

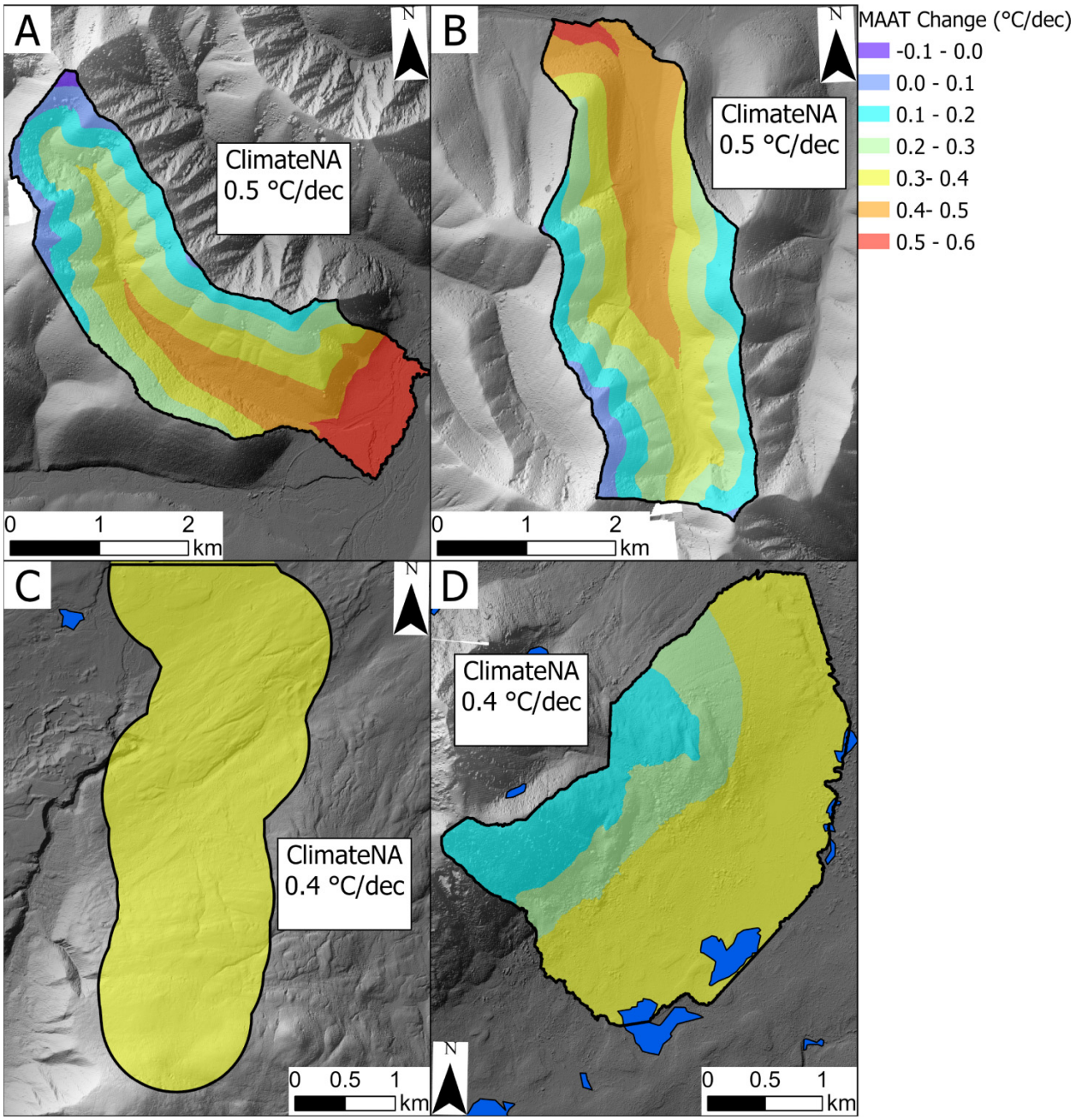

Table 3. Average mean annual air temperature (MAAT) for each of the warming and inversion change scenarios (2071–2100) in the four valleys.

	Current AMAT (°C)	MAAT Constant SLR (°C)	MAAT 1 °C km^{-1} Δ SLR (°C)	MAAT 5 °C km^{-1} Δ SLR (°C)
Valley DS	−6.4	−3.3	−3.5	−4.4
Valley DN	−5.1	−2.1	−2.2	−3.0
Valley M222	−6.2	−3.8	−3.8	−4.0
Valley MTS	−5.1	−2.7	−2.8	−3.1

Note: Annual mean air temperature (AMAT) for current conditions is also given for comparison.

Fig. 5. Spatial distribution of mean annual ground temperature (MAGT) in each of the valleys for current conditions and for the SSP 2–4.5 2071–2100 climate normal assuming no change in the surface lapse rate (SLR), a 1 °C km^{-1} weakening of the inverted SLR, and a 5 °C km^{-1} weakening of the inverted SLR. Base layer from DigitalGlobe Inc. (Imagery © [2017]). Contains information licenced under the Open Government Licence—Canada.

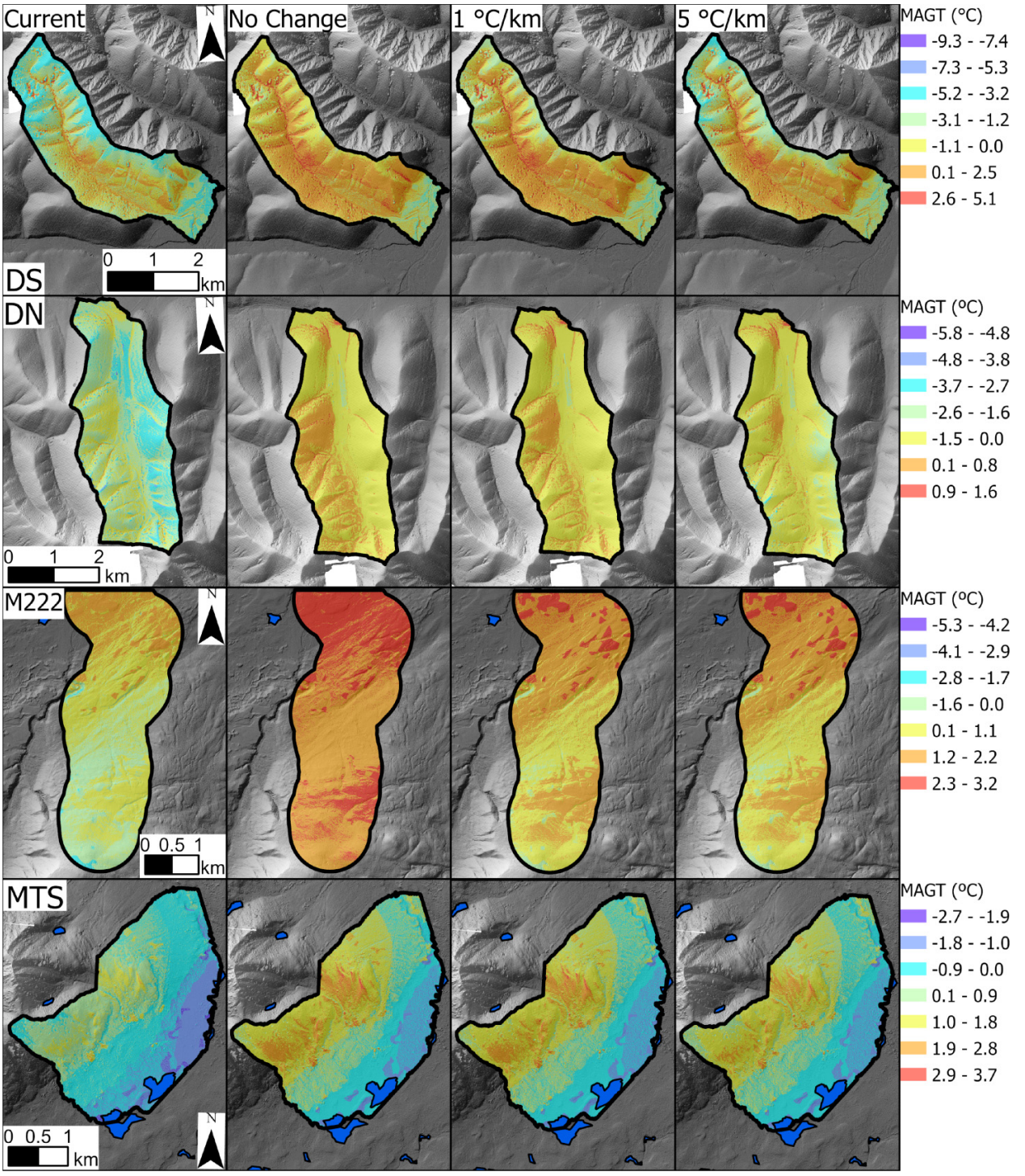

it resulted in the least amount of warming at high elevations (Fig. 6; Table 4). Similarly, the warming scenario with no change in the SLR resulted in the lowest percentage of NSP in each valley due to the increased warming at high elevations. Additionally, this pattern of warming coupled with the original presence of permafrost at both high and low elevations, even in discontinuous permafrost, resulted in the bidirectional spatial loss of NSP in three of the four valleys, Valley DS, Valley DN and Valley MTS. In Valley M222, the loss of NSP was unidirectional as permafrost was only assumed to be present at high elevations under the current climate.

Fig. 6. Near surface permafrost (NSP) presence and absence under the baseline warming with no change in the surface lapse rate (SLR) scenario for (A) Valley DS, (B) Valley DN, (C) Valley M222, and (D) Valley MTS. NSP presence and absence under the baseline warming with a 5 °C km^{-1} weakening of the inverted SLR scenario for (E) Valley DS, (F) Valley DN, (G) Valley M222, and (H) Valley MTS. Thawed NSP indicates the NSP was predicted to thaw between these scenarios and the distribution modelled under the current climate. Base layer from DigitalGlobe Inc. (Imagery © [2017]).

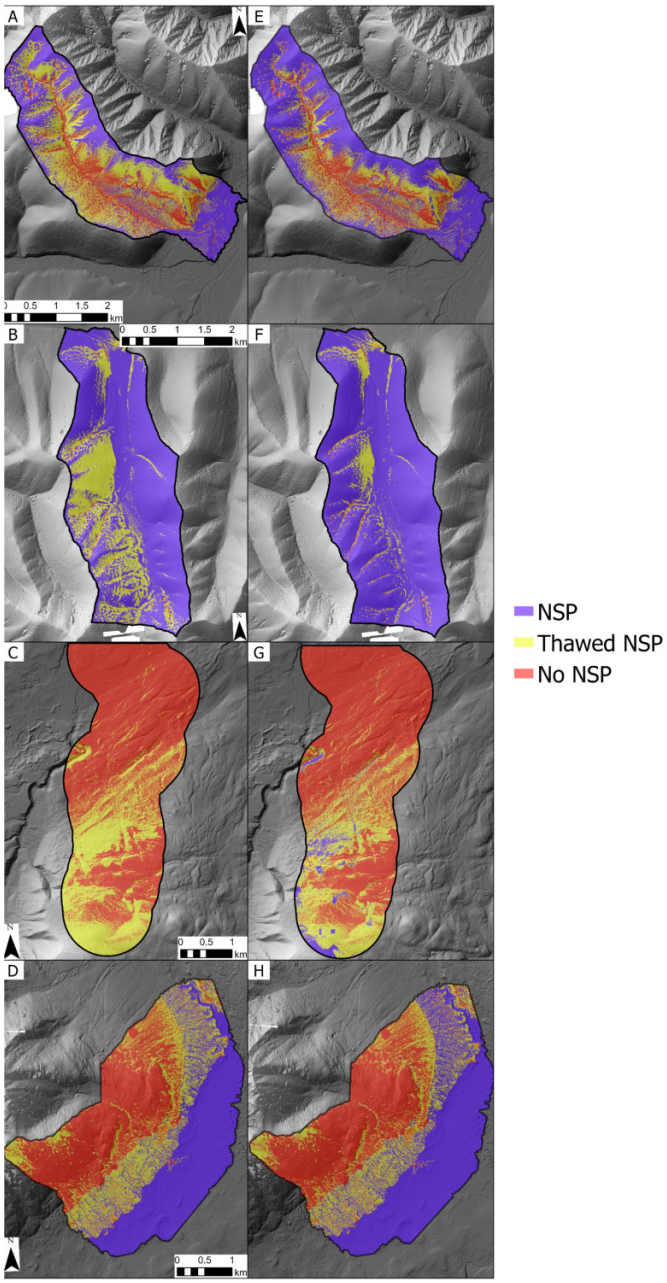

Table 4. Percentage of near surface permafrost (NSP) underlying each valley for the current climate and under each warming scenario.

	Current NSP (%)	Constant SLR (%)	−1 °C km^{-1} Δ SLR (%)	−5 °C km^{-1} Δ SLR (%)
Valley DS	80	42	46	56
Valley DN	99	71	78	90
Valley M222	33	0	3	5
Valley MTS	61	40	40	42

5. Discussion

5.1. Errors and uncertainties

As the models of the future air and ground thermal regime were generated through a scenario-based approach, the exact magnitude of warming at each location is unknown. Additionally, the scenarios used in the study were also based on hypothetical magnitude changes or lack thereof to the strength of the inverted SLR. However, as theorized in several studies, the strength of winter temperature inversions in the Arctic is likely to decrease in a warmer climate due to reduced sea ice extent and increased cloud cover, which prevents the radiative surface cooling required for the formation of strong temperature inversions (Bourne et al. 2010; Screen et al. 2013; Ruman et al. 2022). These mechanisms are also generally responsible for asymmetric climate warming both latitudinally and seasonally whereby temperatures are expected to warm disproportionately at high-latitudes and during winter (Serreze and Barry 2011; IPCC 2022). Although, the temperature inversions in these valleys are primarily radiation based (caused by a lack of solar radiation during winter) and the main factors influencing their presence are not going to change (winter solar radiation and valley geometry), winter air temperatures are expected to be warmer (Wang et al. 2016; Noad and Bonnaventure 2022). Inverted SLRs in Valley DS and Valley DN were more frequently present with colder air temperatures, especially during cold air events (T_a < −30 °C) (Noad and Bonnaventure 2023). As a result, fewer winter cold air events due to generally warmer winter air temperatures may result in less frequent and weaker temperature inversions, decreasing the magnitude of the inverted SLR annually. Therefore, the assumptions made in each scenario regarding changes in SLR strength only in winter (only changing FDD_a) are likely representative of the type of change even if the exact magnitudes used are not accurate. Consequently, although the exact magnitude of warming in both the air and ground for each valley may not be completely certain, the spatial distribution of warming based on changes to the SLR are representative.

Some additional sources of uncertainty arise from assumptions of consistency in n_f, n_t, and rk values through time. This study did not account for changes in precipitation, even though the Arctic is expected to become both warmer and wetter (Boisvert and Stroeve 2015). Changes in precipitation type, timing, and amount will likely alter the effect of changes in air temperature on the ground thermal regime and the n_f values (Krasting et al. 2013). For these valleys snowfall is expected to increase by 38–66 mm (Mahony et al. 2022). However, future n_f values were not perturbed to account for this as they are difficult to predict due the large uncertainties in snowfall redistribution, depth, and morphol-

ogy with climate change, especially in these remote mountain environments (Callaghan et al. 2011; Kapnick and Delworth 2013; Way and Lewkowicz 2016). Additionally changes in snow capture with changing vegetation regimes will also result in warming ground temperatures (Way and Lapalme 2021; Heijmans et al. 2022). However, as the snow redistribution patterns are likely to remain relatively similar (snow will still be scoured from exposed topography or accumulate in hollows) the relative spatial pattern of MAGT is likely accurate even if the exact temperature values for each location are not. Additionally, n_t and rk may vary between the current and future values due to changes in vegetation cover and soil moisture (Andresen et al. 2020; Heijmans et al. 2022). Values of n_t are generally expected to decrease due to changes in vegetation resulting in cooling during the summer (Heijmans et al. 2022). With permafrost thaw, hydrologic pathways and flows are expected to change leading to either drier or wetter surface conditions (Walvoord and Kurylyk 2016; Andresen et al. 2020). Depending on which occurs, the rk value of a location may increase or decrease, with drier conditions resulting in a higher rk (lower differences between frozen and thawed) and wetter conditions decreasing rk values (Burn and Smith 1988; Shiozawa and Campbell 1990). Additionally, future removal of organic layers and moss with fire may increase rk, and result in deeper thaw penetration during the summer, further increasing warming in the ground at depth (Holloway et al. 2020). As with n_f, values of n_t and rk were assumed to remain the same due to the increased complexity in determining the new values and limited knowledge of how they may change locally. This potentially could lead to increased errors in the resulting ground temperature surfaces. As the TTOP model does not directly use surface energy balance terms, variation in the surface energy balance resulting from changes in albedo and cloud cover were not considered, even though these are the main drivers behind EDW (Pepin et al. 2015*b*). However, as the results of this study were mainly to show potential alternatives to EDW based on changes in SLR in high-latitude, continental mountains, direct comparison is not strictly necessary. The inclusion of surface energy balance components to model changes in the air and ground thermal regimes in these regions is an important topic for future work.

5.2. Assessment of EDW in mountains subject to strong temperature inversions

The concept of EDW has been widely tested in low latitude, high elevation mountains dominated by glacial processes (Pepin et al. 2015; Palazzi et al. 2019). The logic and mechanisms behind EDW in these regions are sound, and greater magnitudes of warming at these elevations have been observed (Rangwala and Miller 2010, 2012). A recent evaluation of EDW in the St. Elias Mountains in Yukon also produced evidence of EDW in these high-latitude, maritime mountains with strongly normal SLRs (Williamson et al. 2020). However, as shown through the various warming scenarios in this study, the direct result EDW (greater warming at higher elevations) may not be inclusive of all mountain environments.

In lower elevation, high-latitude mountains subject to annually inverted SLRs, weakening of the SLR in combination with uniform warming potentially results in a greater increase in MAATs in the valley bottom than in high elevations, which may offset warming resulting from the drivers of EDW. Additionally, depending on the magnitude of the weakened SLR, this distribution of warming may propagate to the ground surface and ground at depth. This was shown in a 5 °C km^{-1} SLR weakening scenario as MAGTs were predicted to warm less at high elevations than mid to low elevations. The discrepancy in potential warming patterns is likely a result of the different relations between air temperature and elevation currently present in these valleys compared to those used in the development of EDW. As a result of warming, there are additional possible evolutions to the elevation-MAAT relation that are not present in these low latitude mountains, namely the potential for increasing normality due to warmer overall conditions (Ruman et al. 2022; Noad and Bonnaventure 2023). However, this study did not account for changes in energy balance and therefore did not consider changes in albedo, cloud cover, or latent heat release, all of which are expected to contribute to EDW (Rangwala and Miller 2012; Pepin et al. 2015). As a result, concrete conclusions about the nature (or potential lack) of EDW in these high-latitude, continental mountain environments cannot be made. Instead, potential alternative elevation related warming patterns were demonstrated to allow for refinement of EDW and to highlight a potential complicating factor to better represent a wider variety of mountain environments. Additionally, complexities in the ground thermal response to warming either from changes in SLRs or the traditional drivers of EDW are likely to arise from differences in ground cover and soil properties.

5.3. Differences in warming response between valleys

For each scenario, there were different theoretical warming responses, both within and between valleys, due to ground cover and soil properties. At high elevations and on convex exposed slopes the surface offsets in all valleys were low due to limited vegetation and snow cover (Zhang 2005; Freudiger et al. 2017). As a result, the variability between scenarios was relatively high due to the lack of surface cover, which allowed for a more direct impact of air temperature on the ground thermal regime (Shur and Jorgenson 2007). This shows that ground surface temperatures at these locations are more susceptible to variations in climate driven by changes in SLR or EDW. Contrastingly, ground temperatures varied less between and within scenarios as a result of higher surface offsets and thermal offset due to greater increased snow retention and vegetation cover (Lewkowicz et al. 2012; Bevington and Lewkowicz 2015; Freudiger et al. 2017). Furthermore, increased soil moisture in the valley bottom also may have increased surface offsets (Famiglietti et al.1998; Karunaratne and Burn 2004; Vivoni et al. 2010). On average, Valley DS and Valley DN showed greater subsurface warming than Valley M222 and especially Valley MTS. This is attributed to higher average offsets at Valley M222 and Valley MTS even at the highest elevations, produced by in-

creased snowfall in this region and warmer ground temperatures (Yukon Ecoregions Working Group 2004). Additionally, Valley MTS showed the least amount of warming due to the presence of well-developed vegetation over most of the valley, limiting the ground surface response to changes in air temperature (Viereck 1970; Shur and Jorgenson 2007; Dashtseren et al. 2014; Ran et al. 2021). Moreover, differing surface and thermal offsets in each valley also may have contributed to differences in the spatial pattern of MAGT warming compared to MAAT. In Valley DN, the magnitude and distribution pattern of warming in both the air and ground at depth were similar, especially at high elevations. This results from the dry soil with limited ice content, organic material, or moss cover, especially on the upper slopes, which allows for a more direct connection between the air and ground at depth due to high thermal conductivity during both the thawing and freezing season (Smith and Riseborough 2002; Shur and Jorgenson 2007; Loranty et al. 2018). MAGT in Valley MTS, especially in the valley bottom, did not have a similar spatial distribution pattern or magnitude of warming compared to MAAT. Additionally, the variability between scenarios was limited. The lower portion of Valley MTS is covered by mature forest with a thick moss layer and high soil moisture. This produces differential thermal conductivity seasonally and a high thermal offset, limiting the impact of changing air temperatures on the ground temperature at depth (Loranty et al. 2018). This is also shown in Valley DS, however, there is substantially more variability than Valley MTS, as the ecosystem is less developed in this valley. As a result, high thermal offsets limit the consequences of both warming and changes in temperature inversion strength on the ground temperature at depth, preserving the underlying NSP (Oblogov et al. 2023).

5.4. Differential causes of permafrost thaw

As a result of the differences in MAGT response to warming and subsurface properties, there are likely different drivers of permafrost thaw at different elevations in each valley. Permafrost present at high elevations is largely climate driven, due to the lack of complex ecosystem structure, and its temperature is largely influenced by changes in MAAT (Shur and Jorgenson 2007). Permafrost at these locations is therefore more likely to quickly respond directly to changes in climate (Garibaldi et al. 2021). Due to the presence of mature ecosystems and well-developed organic layers, the permafrost in the valley bottoms, especially in Valley MTS, is likely to be climate driven ecosystem protected. Therefore, permafrost in the valley bottoms is more susceptible to disturbance coupled with warming rather than warming alone, as the permafrost remains protected by the ecosystem properties (Shur and Jorgenson 2007; Daly et al. 2022; Vegter et al. 2024). With the warming projected in this region, it is also likely that this NSP may persist for an extended time beyond 2100, as average MAAT is expected to remain below 0 °C and ecosystem properties have been known to protect permafrost even with MAAT up to + 2 °C (Jorgenson et al. 2010). The permafrost in the valley bottoms also has the potential to be ice rich and contain organic material, yielding a higher likelihood for permafrost thaw manifesting as subsidence and thermokarst (Shur et al. 2005; Kokelj and Jorgenson 2013). This likely poses a greater risk due to the infrastructure present in valley bottoms including roadways and the recently constructed fibre optic line digitally connecting the strategically important location of Inuvik, NT (Dempster Fibre Project 2020).

6. Conclusion

Under a number of potential warming scenarios, MAAT and MAGT showed a variety of responses based on the magnitude and distribution of warming in addition to surface and subsurface characteristics. In all four valleys, warming coupled with weakening inverted SLRs resulted in the greatest increase in MAAT predicted at low elevations. However, under the same scenarios, MAGT showed the greatest warming at high elevations and limited change in the valley bottoms. This discrepancy in warming patterns likely results from variability in surface and thermal offset between the different topographic and vegetation characteristics at the various elevations. Lower elevations were more likely to have lower n_f, n_t, and rk values due to flatter and more incised topography, more mature and complex ecosystem structure, and higher soil moisture. Contrastingly, higher elevations had higher n_f, n_t, and rk values due to more exposed topography, limited to no vegetation, and drier bedrock substrate. As a result, between each scenario, there were larger differences at high elevations, and permafrost was more likely to be preserved in valley bottoms. As permafrost is predicted to be present in the valley bottom and high elevations under each warming scenario, thaw in these valleys is likely to be bidirectional (having fronts moving up and down from mid elevations) rather than unidirectional. This generally supports the concept outlined in the regional permafrost model (Bonnaventure et al. 2012) when subjected to warming conditions outlined by Bonnaventure and Lewkowicz (2013). Additionally, an understanding and inclusion of the spatial distribution of surface and thermal offsets is important for accurate predictions of differential MAGT warming rates and future permafrost distribution due to the resilience of permafrost under well-developed ecosystems as shown in Valley MTS.

Lastly, although the concept of EDW is sound for high elevation mountains with normal SLRs, it may not be entirely representative of the possible warming patterns present in high-latitude continental mountains with intensely inverted SLRs. As a result, EDW should be adjusted to become more inclusive of a wider range of possible spatial warming distributions in distinct mountain environments. This will provide better assessments of warming and potential permafrost thaw and therefore produce more accurate predictions of the subsequent hazards (ground stability and thermokarst) and feedbacks (carbon dioxide and methane release) in environments that are not currently well represented.

Acknowledgements

We acknowledge this research was conducted on the Tr'ondëk Hwëch'in, Acho Dene, and Dehcho First Nation settlement regions and traditional territories. We would like to

thank the many field assistants who aided in the data collection for this research including A. Musk, S. Vegter, and O. Kienzle. Additionally, we acknowledge the funding received through the Natural Science and Engineering Research Council of Canada (NSERC) as well as through the Northern Scientific Training Program (NSTP), through Polar Knowledge Canada and the University of Lethbridge.

Article information

History dates

Received: 1 November 2023
Accepted: 11 June 2024
Accepted manuscript online: 24 June 2024
Version of record online: 14 November 2024

Copyright

Data availability

The in-situ ground and air sensor data used in model creation are available upon request from the corresponding author (madeleine.garibaldi@uleth.ca).

Author information

Author ORCIDs

Madeleine C. Garibaldi https://orcid.org/0000-0001-6801-2743
Philip P. Bonnaventure https://orcid.org/0000-0002-4157-0689
Nick C. Noad https://orcid.org/0000-0003-0652-5337
Will Kochtitzky https://orcid.org/0000-0001-9487-1509

Author contributions

Conceptualization: MCG, PPB
Data curation: MCG
Formal analysis: MCG
Funding acquisition: PPB
Investigation: MCG, PPB, NCN
Methodology: MCG, PPB, NCN
Resources: WK
Software: WK
Supervision: PPB
Visualization: MCG
Writing – original draft: MCG
Writing – review & editing: MCG, PPB, NCN, WK

Competing interests

The authors declare there are no competing interests.

Supplementary material

Supplementary data are available with the article at https://doi.org/10.1139/as-2023-0066.

References

Aguilar-Lome, J., Espinoza-Villar, R., Espinoza, J.-C., Rojas-Acuña, J., Willems, B.L., and Leyva-Molina, W.-M. 2019. Elevation-dependent warming of land surface temperatures in the Andes assessed using MODIS LST time series (2000–2017). International Journal of Applied Earth Observation and Geoinformation, **77**; 119–128. doi:10.1016/j.jag.2018.12.013.

Andresen, C.G., Lawrence, D.M., Wilson, C.J., McGuire, A.D., Koven, C., Schaefer, K., and Zhang, W.,… 2020. Soil moisture and hydrology projections of the permafrost region—a model intercomparison. The Cryosphere, **14**(2): 445–459. doi:10.5194/tc-14-445-2020.

Bevington, A., and Lewkowicz, A.G. 2015. Assessment of a land cover driven TTOP model for mountain and lowland permafrost using field data, southern Yukon and northern British Columbia, Canada. Paper presented at the Proceedings of GéoQuebec: 68th Canadian Geotechnical Conference and 7th Canadian Permafrost Conference. Quebec City, Canada.

Boeckli, L., Brenning, A., Gruber, S., and Noetzli, J. 2012. Permafrost distribution in the European Alps: calculation and evaluation of an index map and summary statistics. The Cryosphere, **6**(4): 807–820. doi:10.5194/tc-6-807-2012.

Boisvert, L.N., and Stroeve, J.C. 2015. The Arctic is becoming warmer and wetter as revealed by the Atmospheric Infrared Sounder. Geophysical Reseach Letters **42(11)**: 4439–4446. doi:10.1002/2015GL063775.

Bonnaventure, P.P., and Lewkowicz, A.G. 2011. Modelling climate change effects on the spatial distribution of mountain permafrost at three sites in northwest Canada. Climate Change, **105**(1): 293–312. doi:10.1007/s10584-010-9818-5.

Bonnaventure, P.P., and Lewkowicz, A.G. 2013. Impacts of mean annual air temperature change on a regional permafrost probability model for the southern Yukon and northern British Columbia, Canada. The Cryosphere, **7**(3): 935–946. doi:10.5194/tc-7-935-2013.

Bonnaventure, P.P., Lewkowicz, A.G., Kremer, M., and Sawada, M.C.A. 2012. Permafrost probability model for the Southern Yukon and Northern British Columbia, Canada. Permafrost and Periglacial Processes, **23**(1): 52–68. doi:10.1002/ppp.1733.

Bostock, H.S. 1966. Notes on glaciation in central Yukon Territory. **Vol. 65**, Department of Mines and Technical Surveys 1966, Ottawa.

Bourne, S.M., Bhatt, U.S., Zhang, J., and Thoman, R. 2010. Surface-based temperature inversions in Alaska from a climate perspective. Atmospheric Research, **95**(2): 353–366. doi:10.1016/j.atmosres.2009.09.013.

Brown, J., Ferrians, O., Heginbottom, J., and Melnikov, E. 2002. Circum-Arctic map of permafrost and ground-ice conditions, version 2. Boulder, Colorado USA, National Snow and Ice Data Center.

Burn, C.R., Moore, J.L., O'Neill, H.B., Hayley, D.W., Trimble, J.R., Calmels, F., et al. 2015. Permafrost Characterization of the Dempster Highway, Yukon and Northwest Territories. Paper presented at the 7th Canadian Permafrost Conference.

Burn, C.R., and Smith, C.A.S. 1988. Observations of the "thermal offset" in near-surface mean annual ground temperatures at several sites near Mayo, Yukon Territory, Canada. Arctic, **41**(2): 99–104. doi:10.14430/arctic1700.

Callaghan, T.V., Johansson, M., Brown, R.D., Groisman, P.Y., Labba, N., Radionov, V., et al. 2011. The changing face of Arctic snow cover: a synthesis of observed and projected changes. Ambio, **40**(Suppl 1): 17–31. doi:10.1007/s13280-011-0212-y.

Daly, S.V., Bonnaventure, P.P., and Kochtitzky, W. 2022. Influence of ecosystem and disturbance on near-surface permafrost distribution, whatì, Northwest Territories, Canada. Permafrost and Periglacial Processes, **33**(4): 339–352. doi:10.1002/ppp.2160.

Dashtseren, A., Ishikawa, M., Iijima, Y., and Jambaljav, Y. 2014. Temperature regimes of the active layer and seasonally frozen ground under a forest-steppe Mosaic, Mongolia. Permafrost and Periglacial Processes, **25**(4): 295–306. doi:10.1002/ppp.1824.

Deluigi, N., Lambiel, C., and Kanevski, M. 2017. Data-driven mapping of the potential mountain permafrost distribution. Science of Total Environment, **590-591**, 370–380; 370-380. doi:10.1016/j.scitotenv.2017.02.041. PMID: 28284636.

Dempster Fibre Project. 2020. Dempster Fibre Project. Available from https://yukon.ca/dempsterfibreproject#current-project-status.

Famiglietti, J.S., Rudnicki, J.W., and Rodell, M., 1998. Variability in surface moisture content along a hillslope transect: Rattlesnake

Hill, Texas. Journal of Hydrology **210**(1-4): 259–281. doi:10.1016/S0022-1694(98)00187-5.

Freudiger, D., Kohn, I., Seibert, J., Stahl, K., and Weiler, M. 2017. Snow redistribution for the hydrological modeling of alpine catchments. WIREs Water **4**(5): e1232. doi:10.1002/wat2.1232.

Garibaldi, M.C., Bonnaventure, P.P., and Lamoureux, S.F. 2021. Utilizing the TTOP model to understand spatial permafrost temperature variability in a High Arctic landscape, Cape Bounty, Nunavut, Canada. Permafrost and Periglacial Processes, **32**(1): 19–34. doi:10.1002/ppp.2086.

Garibaldi, M.C., Bonnaventure, P.P., Noad, N.C., and Kochtitzky, W. 2024. Modelling air, ground surface and permafrost temperature variability across four dissimilar valleys, Yukon, Canada. Arctic Science. doi:10.1139/as-2023-0067.

Garibaldi, M.C., Bonnaventure, P.P., Smith, S.L., and Duchesne, C. 2022. Active layer variability and change in the Mackenzie Valley, Northwest Territories between 1991-2014: an ecoregional assessment. Arctic, Antarctic, and Alpine Research, **54**(1): 274–293. doi:10.1080/15230430.2022.2097156.

Government of Canada. 2015. Canadian Landcover Circa 2000 (Vector)-Geobase Series, 1996-2005. Natural Resources Canada. Available from https://open.canada.ca/data/en/dataset/97126362-5a85-4fe0-9dc2-915464cfdbb7 [accessed May 2019] </Dataset>.

Government of Canada. 2016. Coastal Waters (polygons), Boundary Files –2016 Census. Statistics Canada. Available from https://open.canada.ca/data/en/dataset/6c78fb2f-d23b-45b4-b3af-cc6f6cc4fff8 [accessed September 2019] </Dataset>.

Government of Canada. 2016. Provinces/Territories Cartographic Boundary File –2016 Census. Statistics Canada. Available from https://open.canada.ca/data/en/dataset/a883eb14-0c0e-45c4-b8c4-b54c4a819edb [accessed September 2019] </Dataset>.

Government of Canada. 2017. Lakes, Rivers, and Glaciers in Canada—Canvec Series—Hydrographic Features. Natural Resources Canada. Available from https://open.canada.ca/data/en/dataset/9d96e8c9-22fe-4ad2-b5e8-94a6991b744b [accessed April 2019] </Dataset>.

Government of Canada. 2017. Transport Networks in Canada—Canvec Series—Transport Features. Transport Canada. Available from https://open.canada.ca/data/en/dataset/c5c249c4-dea6-40a6-8fae-188a42030908 [accessed January 2019] </Dataset>.

Government of United States. 2018. Cartographic Boundary Files—Shapefiles -cb_2018_us_state_20 m. United States Census Bureau. Available from https://www.census.gov/geographies/mapping-files/time-series/geo/carto-boundary-file.html [accessed September 2019] </Dataset>.

Government of Yukon. 2021. Yukon Communities. Geomatics Yukon. Available from https://open.yukon.ca/data/datasets/yukon-communities [accessed June 2022] </Dataset>.

Gruber, S., and Haeberli, W. 2009. Mountain permafrost. Permafrost Soils, 33–44. doi:10.1007/978-3-540-69371-0_3.

Guglielmin, M., Aldighieri, B., and Testa, B. 2003. PERMACLIM: a model for the distribution of mountain permafrost, based on climatic observations. Geomorphology, **51**(4): 245–257. doi:10.1016/S0169-555X(02)00221-0.

Harris, C., Arenson, L.U., Christiansen, H.H., Etzelmüller, B., Frauenfelder, R., Gruber, S., et al. 2009. Permafrost and climate in Europe: monitoring and modelling thermal, geomorphological and geotechnical responses. Earth-Science Reviews, **92**(3): 117–171. doi:10.1016/j.earscirev.2008.12.002.

Heginbottom, J. 1995. Canada, permafrost: Canada Map Office.

Heijmans, M.M.P.D., Magnússon, R.Í., Lara, M.J., Frost, G.V., Myers-Smith, I.H., van Huissteden, J., and Limpens, J.,… 2022. Tundra vegetation change and impacts on permafrost. Nature Reviews Earth & Environment, **3**(1): 68–84. doi:10.1038/s43017-021-00233-0.

Holloway, J.E., Lewkowicz, A.G., Douglas, T.A., Li, X., Turetsky, M.R., Baltzer, J.L., and Jin, H. 2020. Impact of wildfire on permafrost landscapes: a review of recent advances and future prospects. Permafrost and Periglacial Processes, **31**(3): 371–382. doi:10.1002/ppp.2048.

Hou, P., and Wu, S. 2016. Long-term changes in extreme air pollution meteorology and the implications for air quality. Scientific Reports, **8**(1): 1–7. doi:10.1038/s41598-018-33214-3.

IPCC. 2022. Climate Change 2022: impacts, adaptation and vulnerability. In Contribution of Working Group II to the Sixth Assessment Report of the Intergovernmental Panel on Climate Change. Edited by H.-O. Pörtner, D.C. Roberts, M. Tignor, E.S. Poloczanska, K. Mintenbeck, A. Alegría , et al., Cambridge University Press, Cambridge, UK and New York, NY, USA. p. 3056. doi:10.1017/9781009325844.

Jorgenson, M.T., Romanovsky, V., Harden, J., Shur, Y., O'Donnell, J., Schuur, E.A.G., and Marchenko, S.,… 2010. Resilience and vulnerability of permafrost to climate change. Canadian Journal of Forest Research, **40**(7): 1219–1236. doi:10.1139/X10-060.

Kapnick, S.B., and Delworth, T.L. 2013. Controls of global snow under a changed climate. Journal of Climate, **26**(15): 5537–5562. doi:10.1175/JCLI-D-12-00528.1.

Karunaratne, K.C., and Burn, C.R. 2004. Relations between air and surface temperature in discontinuous permafrost terrain near Mayo, Yukon Territory. Canadian Journal of Earth Sciences **41**(12): 1437–1451. doi:10.1139/e04-082.

Koenigk, T., Brodeau, L., Graversen, R.G., Karlsson, J., Svensson, G., Tjernström, M., et al. 2013. Arctic climate change in 21st century CMIP5 simulations with EC-Earth. Climate Dynamics, **40**(11): 2719–2743. doi:10.1007/s00382-012-1505-y.

Kokelj, S.V., and Jorgenson, M.T. 2013. Advances in thermokarst research. Permafrost and Periglacial Processes, **24**(2): 108–119. doi:10.1002/ppp.1779.

Krasting, J.P., Broccoli, A.J., Dixon, K.W., and Lanzante, J.R. 2013. Future changes in Northern Hemisphere snowfall. Journal of Climate, **26**(20): 7813–7828. doi:10.1175/JCLI-D-12-00832.1.

Lewkowicz, A.G., and Bonnaventure, P.P. 2011. Equivalent elevation: a new method to incorporate variable surface lapse rates into mountain permafrost modelling. Permafrost and Periglacial Processes, **22**(2): 153–162. doi:10.1002/ppp.720.

Lewkowicz, A.G., Bonnaventure, P.P., Smith, S.L., and Kuntz, Z. 2012. Spatial and thermal characteristics of mountain permafrost, northwest canada. Geografiska Annaler: Series A, Physical Geography, **94**(2): 195–213. doi:10.1111/j.1468-0459.2012.00462.x.

Li, B., Chen, Y., and Shi, X. 2020. Does elevation dependent warming exist in high mountain Asia? Environmental Research Letters, **15**(2): 024012. doi:10.1088/1748-9326/ab6d7f.

Loranty, M.M., Abbott, B.W., Blok, D., Douglas, T.A., Epstein, H.E., Forbes, B.C., et al. 2018. Reviews and syntheses: changing ecosystem influences on soil thermal regimes in northern high-latitude permafrost regions. Biogeosciences, **15**(17): 5287–5313. doi:10.5194/bg-15-5287-2018.

Mahony, CR., Wang, T., Hamann, A., and Cannon, A.J. 2022. A CMIP6 ensemble for downscaled monthly climate normals over North America. International Journal of Climatology, **42**(11): 5871–5891. doi:10.1002/joc.7566.

Minder, J.R., Letcher, T.W., and Liu, C. 2018. The character and causes of elevation-dependent warming in high-resolution simulations of Rocky Mountain climate change. Journal of Climate, **31**(6): 2093–2113. doi:10.1175/JCLI-D-17-0321.1.

Mountain Research Initiative Edw Working Group.Pepin, N. Bradley, R.S., Diaz, H.F., Baraer, M., Caceres, E.B., and Forsythe, N., 2015. levation-dependent warming in mountain regions of the world. Nature Climate Change, **5**(5): 424–430. doi:10.1038/nclimate2563.

Nitzbon, J., Westermann, S., Langer, M., Martin, L.C.P., Strauss, J., Laboor, S., and Boike, J. 2020. Fast response of cold ice-rich permafrost in northeast Siberia to a warming climate. Nature Communications, **11**(1): 2201. doi:10.1038/s41467-020-15725-8.

Noad, N.C., and Bonnaventure, P.P. 2022. Surface temperature inversion characteristics in dissimilar valleys, Yukon Canada. Arctic Science, **8**(4): 1320–1339.

Noad, N.C., and Bonnaventure, P.P. 2023. Examining the influence of microclimate conditions on the breakup of surface-based temperature inversions in two proximal but dissimilar Yukon valleys. The Canadian Geographer/Le Géographe canadien.

O'Neill, H.B., Wolfe, S.A., and Duchesne, C. 2019. New ground ice maps for Canada using a paleogeographic modelling approach. The Cryosphere, **13**(3): 753–773. doi:10.5194/tc-13-753-2019.

Oblogov, G.E., Vasiliev, A.A., Streletskiy, D.A., Shiklomanov, N.I., and Nyland, K.E. 2023. Localized vegetation, soil moisture, and ice content offset permafrost degradation under climate warming. Geosciences, **13**(5): 129. doi:10.3390/geosciences13050129.

Palazzi, E., Mortarini, L., Terzago, S., and Von Hardenberg, J. 2019. Elevation-dependent warming in global climate model simulations

at high spatial resolution. Climate Dynamics, **52**(5): 2685–2702. doi:10.1007/s00382-018-4287-z.

Ran, Y., Jorgenson, M.T., Li, X., Jin, H., Wu, T., Li, R., and Cheng, G. 2021. Biophysical permafrost map indicates ecosystem processes dominate permafrost stability in the Northern Hemisphere. Environmental Research Letters, **16**(9): 095010. doi:10.1088/1748-9326/ac20f3.

Rangecroft, S., Suggitt, A.J., Anderson, K., and Harrison, S. 2016. Future climate warming and changes to mountain permafrost in the Bolivian Andes. Climate Change, **137**(1): 231–243. doi:10.1007/s10584-016-1655-8.

Rangwala, I., and Miller, J.R. 2010. Twentieth century temperature trends in Colorado's San Juan Mountains. Arctic, Antarctic, and Alpine Research **42**(1): 89–97. doi:10.1657/1938-4246-42.1.89.

Rangwala, I., and Miller, J.R. 2012. Climate change in mountains: a review of elevation-dependent warming and its possible causes. Climate Change, **114**(3): 527–547. doi:10.1007/s10584-012-0419-3.

Ruman, C.J., Monahan, A.H., and Sushama, L. 2022. Climatology of Arctic temperature inversions in current and future climates. Theoretical and Applied Climatology, **150**(1): 121–134. doi:10.1007/s00704-022-04147-9.

Screen, J.A., Simmonds, I., Deser, C., and Tomas, R. 2013. The atmospheric response to three decades of observed Arctic Sea ice loss. Journal of Climate, **26**(4): 1230–1248. doi:10.1175/JCLI-D-12-00063.1.

Serreze, M.C., and Barry, R.G. 2011. Processes and impacts of Arctic amplification: a research synthesis. Global and Planetary Change, **77**(1): 85–96. doi:10.1016/j.gloplacha.2011.03.004.

Shiozawa, S., and Campbell, G.S. 1990. Soil thermal conductivity. Remote Sensing Reviews, **5**(1): 301–310. doi:10.1080/02757259009532137.

Shur, Y., Hinkel, K.M., and Nelson, F.E. 2005. The transient layer: implications for geocryology and climate-change science. Permafrost and Periglacial Processes, **16**(1): 5–17. doi:10.1002/ppp.518.

Shur, Y.L., and Jorgenson, M.T. 2007. Patterns of permafrost formation and degradation in relation to climate and ecosystems. Permafrost and Periglacial Processes, **18**(1): 7–19. doi:10.1002/ppp.582.

Smith, M.W., and Riseborough, D.W. 2002. Climate and the limits of permafrost: a zonal analysis. Permafrost and Periglacial Processes, **13**(1): 1–15. doi:10.1002/ppp.410.

Soong, J.L., Phillips, C.L., Ledna, C., Koven, C.D., and Torn, M.S. 2020. CMIP5 Models predict rapid and deep soil warming over the 21st century. Journal of Geophysical Research: Biogeosciences, **125**(2): e2019JG005266. doi:10.1029/2019JG005266.

Vegter, S., Bonnaventure, P.P., Daly, S., and Kochtitzky, W. 2024. Modelling permafrost distribution using the temperature at top of permafrost model in the Boreal forest environment of Whatì, NT. Arctic Science. doi:10.1139/AS-2023-0010.

Viereck, L.A. 1970. Forest succession and soil development adjacent to the Chena River in Interior Alaska. Arctic and Alpine Research, **2**(1): 1–26. doi:10.1080/00040851.1970.12003558.

Vivoni, E.R., Rodriguez, J.C., and Watts, C.J. 2010. On the spatiotemporal variability of soil moisture and evapotranspiration in a mountainous basin within the North American monsoon region. Water Resources Research, **46** (2). doi: 10.1029/2009WR008240.

Walvoord, M.A., and Kurylyk, B.L. 2016. Hydrologic impacts of thawing Permafrost—a review. Vadose Zone Journal, 1–20, **15**(6). doi:10.2136/vzj2016.01.0010.

Wang, T., Hamann, A., Spittlehouse, D., and Carroll, C. 2016. Locally downscaled and spatially customizable climate data for historical and future periods for North America. PLoS One, **11**(6): e0156720. doi:10.1371/journal.pone.0156720.

Way, R.G., and Lapalme, C.M. 2021. Does tall vegetation warm or cool the ground surface? Constraining the ground thermal impacts of upright vegetation in northern environments. Environmental Research Letters, **16**(5): 054077. doi:10.1088/1748-9326/abef31.

Way, R.G., and Lewkowicz, A.G. 2016. Modelling the spatial distribution of permafrost in Labrador–Ungava using the temperature at the top of permafrost. Canadian Journal of Earth Sciences, **53**(10): 1010–1028. doi:10.1139/cjes-2016-0034.

Williamson, S.N., Zdanowicz, C., Anslow, F.S., Clarke, G.K., Copland, L., Danby, R.K., and Hik, D.S.,… 2020. Evidence for elevation-dependent warming in the St. Elias Mountains, Yukon, Canada. Journal of Climate, **33**(8): 3253–3269. doi:10.1175/JCLI-D-19-0405.1.

You, Q., Kang, S., Pepin, N., Flügel, W.-A., Yan, Y., Behrawan, H., and Huang, J. 2010. Relationship between temperature trend magnitude, elevation and mean temperature in the Tibetan Plateau from homogenized surface stations and reanalysis data. Global and Planetary Change, **71**(1-2): 124–133. doi:10.1016/j.gloplacha.2010.01.020.

Yukon Ecoregions Working Group. 2004. Yukon Coastal Plain. *In* Ecoregions of the Yukon Territory: Biophysical properties of Yukon landscapes. Edited by C.A.S. Smith, J.C. Meikle and C.F. Roots, Agriculture and Agri-Food Canada, PARC Technical Bulletin No. 04-01, Summerland, British Columbia, p. 63–72.

Zhang, G., Mu, C., Nan, Z., Wu, X., and Cheng, G. 2023. Elevation dependency of future degradation of permafrost over the Qinghai-Tibet Plateau. Environmental Research Letters.

Zhang, T. 2005. Influence of the seasonal snow cover on the ground thermal regime: an overview. Reviews of Geophysics, **43**(4): n/a–n/a. doi:10.1029/2004RG000157.

Zhang, Y., Seidel, D.J., Golaz, J.C., Deser, C., and Tomas, R.A. 2011. Climatological characteristics of Arctic and Antarctic surface-based inversions. Journal of Climate, **24**(19): 5167–5186. doi:10.1175/2011JCLI4004.1.